Phase properties of several nonlinear optical waves described by rational solutions

Jia-Dong Li, Ling-Zheng Meng, and Li-Chen Zhao*
School of Physics, Northwest University, Xi'an 710127, China;
Peng Huanwu Center for Fundamental Theory, Xi'an 710127, China;
and Shaanxi Key Laboratory for Theoretical Physics Frontiers, Xi'an 710127, China

(Received 24 August 2022; revised 12 November 2022; accepted 5 January 2023; published 18 January 2023)

Phase plays an essential role in both classical and quantum wave dynamics, which has motivated many scientists to study the phases of many different nonlinear waves. Among those nonlinear waves, the ones described by rational solutions have been given much attention, partly because some of them can describe rogue wave dynamics. We revisit the phase of several well-known one-dimensional rational solutions and clarify that sudden phase inversion processes indeed exist for rogue waves, in contrast to the ones reported before. Moreover, we investigate the phase properties of rogue waves and rational W-shaped solitons in the Hirota and Sasa-Satsuma model, for which some high-order physical effects are considered, i.e., the third-order dispersion delayed nonlinear response and self-steeping effects. The quite distinctive phases are uncovered for the rational W-shaped solitons with similar density profiles in the two models, by limitation analysis on the underlying topological vector potentials of other related nonlinear waves. These results indicate that the underlying topological vector potentials can be used to identify the phases of nonlinear waves, especially for localized waves with abrupt phase jumps.

DOI: 10.1103/PhysRevA.107.013511

I. INTRODUCTION

Phase is one of the most important properties of nonlinear waves, because it plays an essential role in both classical and quantum wave dynamics. This has motivated many scientists to study the phases of many different nonlinear waves, such as bright solitons [1], dark solitons [2], Akhmediev breathers [3], Kuznetsov-Ma breathers [4,5], and rogue waves (RWs) [6]. For example, a dark soliton usually admits a phase jump across its density dip, and the relative phase between bright solitons plays an important role in their interaction behaviors. The Akhmediev breather usually possesses a phase shift of its plane wave background [7,8], which could be seen as a nonlinear geometric phase. For the Peregrine RW, two sharp π phase jumps can be seen when the density peak admits the maximum value [8–14]. Systemic analysis was performed on phase evolution of RWs and high-order RWs [8,9], based on related rational solutions of integrable nonlinear partial equations. We note that the phases of the identical first-order RW were different between Ref. [8] and Ref. [9]. The phases of high-order RWs given in Ref. [9] have no phase inversion process, in contrast to the ones in Ref. [15]. Considering that the relative phase evolution in the temporal-spatial plane should be unique with choosing a reference state [16], we would like to revisit the phase of RWs and other related nonlinear waves described by rational solutions.

The phase of wave function ψ can be generally described by the arctan $\left[\frac{\mathrm{Im}[\psi]}{\mathrm{Re}[\psi]}\right] + n\pi$ or other arccosine forms (where n is an integer and is determined by the phase gradient direction). But this form cannot deal with the cases with abrupt phase jumps, since the phase gradient becomes divergent on the abrupt phase jump point. This means the mathematical forms usually cannot identify a phase uniquely and correctly, especially for the real functions with many nodes (each node with $\pm\pi$ phase jump) and wave functions with some abrupt 2π phase jumps. Note that the phase jump direction can be chosen arbitrarily if we just observe the phase at one moment, but the phase jumps should be unique when investigating the relative phase on the whole temporal-spatial plane. For example, the $\pi \to -\pi$ phase jump along the evolution direction for the first-order RW cannot be seen from the mathematical phase form, but its existence plays an important role in its amplitude decay dynamics [10,14,15]. How to identify the phase of waves with abrupt phase jumps physically and conveniently is still a challenging problem.

In this paper, we suggest that the relative phase can be determined uniquely based on the general phase form, with the aid of investigating the topological vector potential underlying nonlinear waves [15,17]. The topological vector potential can be given from the analytic complex extension of the phase gradient function. The limitation analysis of topological vector potential can be used to determine the phase distribution and evolution when there are abrupt phase jumps. We investigate the phase properties of several one-dimensional nonlinear waves with the aid of topological vector potentials. The abrupt phase jump $j\pi \to -j\pi$ ($j = 1, 2, 3$ is the order of RW) is uncovered for the first-, second-, and third-order RWs when the density peak possesses the maximum value. Moreover, the phase properties of RWs and rational W-shaped solitons in the Hirota and Sasa-Satsuma (S-S) models are analyzed in detail, which uncovers the quite distinctive phases for the

*zhaolichen3@nwu.edu.cn

rational W-shaped solitons with similar density profiles in the two models.

The paper is organized as follows. We analyze the phase of the first-, second-, and third-order RWs of the simplest nonlinear Schrödinger equation (NLSE) model in Sec. II. In Sec. III, we calculate the phase of RWs and rational W-shaped solitons in the Hirota model and the S-S model. We show that their phases are quite distinctive even though they admit similar density profiles. A conclusion is made in Sec. IV.

II. ROGUE WAVE PHASE OF THE SIMPLEST NONLINEAR SCHRÖDINGER EQUATION

We choose one of the simplest models, the scalar NLSE, to discuss the phase of nonlinear waves. It can be written as

$$i\frac{\partial\psi}{\partial z}+\frac{1}{2}\frac{\partial^2\psi}{\partial t^2}+|\psi|^2\psi=0, \tag{1}$$

where t is the retarded time and z is the propagation distance for nonlinear optical fiber systems [18]. The above model admits bright solitons, Akhmediev breathers, Kuznetsov-Ma breathers, and RWs [3–6,19–21]. Those nonlinear waves have different structures and periodic properties. Especially, they exhibit distinctive phases, which is highly correlated with their density evolution [7,8]. For the RW, when its amplitude reaches the maximum value, the phase increases rapidly and a localized π phase jump occurs. Experimental observation has been done for the first-order RWs and some high-order RWs [10], which provides possibilities to observe the phase evolution on the spatial-temporal plane. Noting that there were several different phase characterizations for the identical RWs [8,9,15], we revisit the phase of RWs with the aid of topological vector potentials, which reveals the topology underlying the phase jumps of dark solitons [17].

A. The phases of the first-order rogue waves

The first-order RW solution can be written as

$$\psi=\left[1-\frac{4(1+2iz)}{4z^2+4t^2+1}\right]e^{iz}, \tag{2}$$

whose dynamics process is shown in Fig. 1(a) [22,23]. The amplitude peak is located at $t=0$, and on either side of the peak, there are two valleys at $t=\pm a_0$ ($a_0=\frac{\sqrt{3}}{2}$). Many theoretical and experimental investigations have been done on the phases of RWs [7–10,12–14,19]. Recently, we showed that the first-order RW admitted several phase jumps and a sudden phase inversion [15], which is completely different from the other previous studies [8,9]. We discuss the phases of RWs in more detail to clarify the differences.

In order to obtain the actual phase evolution of nonlinear waves, the phase gradient flow $F(t)=\frac{d\phi(t,z)}{dt}$ must be considered. Here, $\phi(t,z)$ denotes the phase of the RW, for which the global trivial phase of the background (the factor e^{iz}) is removed, in order to investigate the phase evolution of RWs more conveniently. Noting that density zeros play an important role in phase jumps, we analytically extend the function $F(t)$ to be $F(m)$, replacing t with $m=t+i\tau$, to investigate density zeros on the complex plane. We can see that $F(m)$ has four singularities, i.e., $m_{1,2}=t_{1,2}+i\tau_{1,2}=\pm(a+ib)$ and $m_{3,4}=t_{3,4}+i\tau_{3,4}=\pm(a-ib)$, where $a=\frac{2\sqrt{2}z}{\sqrt{4z^2+\sqrt{16z^4+40z^2+9}-3}}$ and $b=\frac{\sqrt{4z^2+\sqrt{16z^4+40z^2+9}-3}}{2\sqrt{2}}$. Then we can define a vector potential $\mathscr{A}_c=\frac{\partial\phi(m,z)}{\partial t}\mathbf{e}_t+\frac{\partial\phi(m,z)}{\partial\tau}\mathbf{e}_\tau$ on the complex plane $(t,i\tau)$, where $\mathbf{e}_t$ and $\mathbf{e}_\tau$ are the unit vectors along the t and τ directions, respectively. The real part of the above vector potential, i.e., $\mathbf{A}=\mathrm{Re}[\mathscr{A}_c]$, can be derived as [15]

$$\mathrm{A}=\sum_{N=1}^{4}\frac{\pm\pi[(t-t_N)\mathbf{e}_\tau-(\tau-\tau_N)\mathbf{e}_t]}{2\pi[(t-t_N)^2+(\tau-\tau_N)^2]}. \tag{3}$$

The $\pm$ can be known directly from the residue of each singularity for $F(m)$. The topological vector potential describes four Dirac monopoles, which locate on density zeros on the complex plane. The relative phase variation can be described by the integration of the vector potential $\mathbf{A}$ along the real t axis. Recently, wavefront dislocation and phase singularity of several nonlinear waves were discussed [24,25], for which topology is defined on the spatial-temporal plane. The phase singularities locate at density zeros on the real spatial-temporal plane, which could be understood from the density zeros on the extended complex plane. The relations between topologies on the different spaces still need further research. In this paper, we mainly intend to identify the relative phase of rogue waves with the aid of these topological vector potentials on the complex plane.

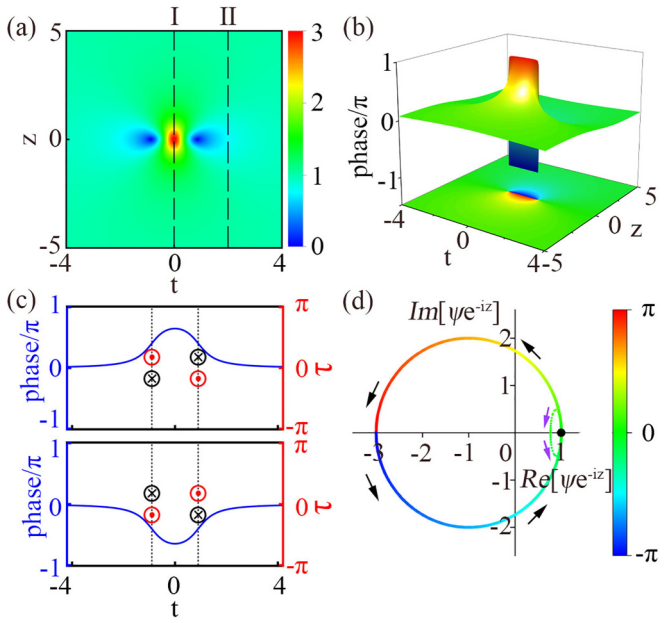

FIG. 1. (a) The amplitude evolution of the first-order RW solution. (b) The corresponding phase evolution. (c) The virtual monopoles distribution on the extended complex plane and phase distribution before (z = -0.5) and after (z = 0.5) the highest peak emerging. The monopoles with positive and negative charges (i.e., $\pm\frac{1}{2}$) are indicated by $\odot$ and $\otimes$, respectively. (d) Phase-diagram trajectories on the ($\mathrm{Re}[\psi e^{-iz}]$, $\mathrm{Im}[\psi e^{-iz}]$) space of the first-order RW wave function at $t=0$ (I) and $t=2$ (II). The black dot indicates the starting and ending positions. The evolution directions at I and II are marked by black arrows and purple arrows, respectively. The dashed square indicates the position of phase inversion $\pi\rightarrow-\pi$.

But the wave function becomes real when $z = 0$, which makes it difficult to fix the phase at this moment. We can deal with the case by taking limitation analysis on the above vector potential. As $z \to \pm 0$, $a \to \pm a_0$ and $b \to 0$. The vector potential on the real axis then takes the following form:

$$\lim_{z\to\pm 0} \mathbf{A} = \lim_{b\to 0} \left\{ \frac{-\pi[(t \pm a_0)\mathbf{e}_\tau + b\mathbf{e}_t]}{2\pi[(t \pm a_0)^2 + b^2]} + \frac{\pi[(t \pm a_0)\mathbf{e}_\tau - b\mathbf{e}_t]}{2\pi[(t \pm a_0)^2 + b^2]} + \frac{\pi[(t \mp a_0)\mathbf{e}_\tau + b\mathbf{e}_t]}{2\pi[(t \mp a_0)^2 + b^2]} + \frac{-\pi[(t \mp a_0)\mathbf{e}_\tau - b\mathbf{e}_t]}{2\pi[(t \mp a_0)^2 + b^2]} \right\} = (-\pi\delta[t \pm a_0] + \pi\delta[t \mp a_0])\,\mathbf{e}_t. \quad (4)$$

The line integral of the above vector potential along the real axis predicts the π phase jumps and abrupt phase inversion ($\pi \to -\pi$ phase jump). The vector potential composed of oppositely charged monopoles can fully capture the fundamental features of the nonlinear wave's phase evolution [15,17,26].

We note that the relative phase evolution should be uniquely determined in the temporal-spatial plane, although the phase of a single point can be chosen arbitrarily. Therefore, we plot the phase evolution of the first-order RW, fixing a reference state. For simplicity and without losing generality, we choose ψ at $z \to -\infty$ as the reference state [16], namely, $\phi(t, z \to -\infty) = 0$, to determine the phase of RW. Judging the phase gradient flow and taking the limitation analysis on vector potential [see Eq. (4)], we plot the phase evolution of the first-order RW [shown in Fig. 1(b)], based on the general $\arctan\left[\frac{\mathrm{Im}[\psi e^{-iz}]}{\mathrm{Re}[\psi e^{-iz}]}\right] + n\pi$ form. One can find that the phase grows from zero to a π jump as the peak of the RW is compressed. Then it shows a sudden phase jump $\pi \to -\pi$, which is somewhat similar to the cases reported in linear optic waves [16,27]. Phase bifurcations are marked by zero-amplitude troughs, as pointed out in Ref. [9]. After that, the phase gradually tends to zero, and the corresponding density decreases to be identical to the plane wave background. The phase gradient determines the density flow, and the abrupt phase inversion in the phase distribution can provide an understanding of the growth and decay of RWs. Our results are in sharp contrast to Fig. 1(c) of Ref. [9], in which the RW phase evolves without inversion and it cannot explain the RW's amplitude decay process. Our results are also different from the ones in Fig. 6 of Ref. [8], in which the 2π phase jump was admitted by the RW's plane wave background, and the local phase of the RW evolved continuously. In fact, the phase of the first-order RW cannot be determined uniquely when it admits the highest peak [at $z = 0$ in Fig. 1(b)], since the phase for waves in regime $[-a_0, a_0]$ along the z direction is discontinuous at the point $z = 0$. In the experiment of measuring the RW's phase (i.e., Fig. 3(c) in Ref. [10]), we think that the phase was measured at the distance slightly before the RW's highest peak appearing.

From the vector potential characters, we know that in addition to these singular points, the corresponding magnetic field is zero everywhere in the whole complex plane. That is,

$$\mathrm{B} = \mathbf{e}_k \sum_N \pm\pi\delta[\mathbf{m} - \mathbf{m}_N], \quad (5)$$

where $\mathbf{m}$ is the vector on (t, τ) plane, and $\mathbf{e}_k$ is a unit vector which is perpendicular to the (t, τ) plane. The $\pm$ represents the magnetic flux direction. Each singularity in the vector potential forms a monopole field with an elementary π quantized magnetic flux. We show the monopole field at two different distances in Fig. 1(c). Each pair of oppositely charged monopoles in the vertical direction approaches the other and results in more sharp phase changes. At $z = 0$, the two pairs collide, which results in the two π phase jumps. Then they bounce back after exchanging charges, and the phase jump direction abruptly inverses. As the monopoles move away, the phase of RW returns to zero.

To understand the differences between our results and the ones in Refs. [8,9], it is meaningful to investigate the trajectories of wave function on the complex plane [28]. We plot the trajectories of ψe^{-iz} and the corresponding phases at $t = 0$ (denoted by I) and $t = 2$ (denoted by II) with propagation distance on the $(\mathrm{Re}[\psi e^{-iz}], \mathrm{Im}[\psi e^{-iz}])$ plane, which are shown in Fig. 1(d). We can see that our phase at $t = 0$ first increases and reaches π at $z = 0$, then presents an abrupt inversion to $-\pi$ and continues to increase, and finally it returns to zero. If we just observe trajectory I on the $(\mathrm{Re}[\psi e^{-iz}], \mathrm{Im}[\psi e^{-iz}])$ plane, the circle around the coordinate origin suggests that the phase should admit a 2π phase difference compared to the initial state. This indicates that a 2π phase evolution was argued to be possessed continuously by the RW signal, and the RW's background was suggested to admit an abrupt 2π phase jump (see Fig. 6 in Ref. [8]). The abrupt 2π phase jump possessed by RW's background can make the phase gradient agree with the density flow during the RW's decay process. However, we argue that the 2π phase difference is possessed only by the RW signal, which is hidden in the $\pi \to -\pi$ phase jump [see the dashed square in Fig. 1(d)]. The abrupt $\pi \to -\pi$ phase jump makes the RW's initial phase ($z \to -\infty$) equal to the final phase ($z \to \infty$), in sharp contrast to the ones in Ref. [8]. Especially, we think that there is no phase jump for the RW's plane wave background, which is supported by the trajectories far from the RW's hump and valleys. For the phase at $t = 2$ [trajectory II in Fig. 1(d), which is outside the two valleys], the small circle is not around the coordinate origin, and there should be no phase difference between the initial state and final state. If we further investigate the phase at $t \to \infty$, the trajectory is continuously reduced to one point, which is far from the coordinate origin. Therefore, there should be no phase change for RW's plane wave background.

On the other hand, the phase of RW's plane wave background was also suggested to admit no variations, and the 2π phase difference was continuously possessed by RW, see Fig. 1(c) in Ref. [9]. The difference between the RW peak's initial phase ($z \to -\infty$) and the final phase ($z \to \infty$) was 2π, in contrast to our zero phase difference. This indicates that the plane wave background admits two striking 2π phase jump points along the distribution direction after the highest density peak emerges. Considering that the RW localizes at the temporal-spatial plane, we think that the abrupt $\pi \to -\pi$ phase jump should be more naturally possessed by the RW signal. This ensures that the whole plane wave background admits no phase variations. Our results are also helpful in understanding the differences between Refs. [8] and [9] for the identical RWs.

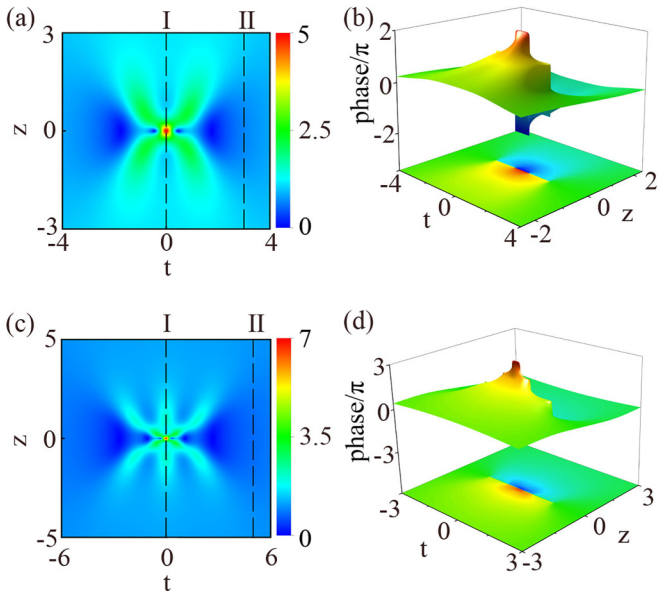

FIG. 2. (a) and (b) The amplitude and phase evolution of the second-order RW solution. There are two abrupt phase jumps ($2\pi \to -2\pi$ and $\pi \to -\pi$) in the phase evolution of the second-order RWs. (c) and (d) The amplitude and phase evolution of the third-order RW solution. There are three abrupt phase jumps ($3\pi \to -3\pi$, $2\pi \to -2\pi$, and $\pi \to -\pi$) in the phase evolution of the third-order RWs.

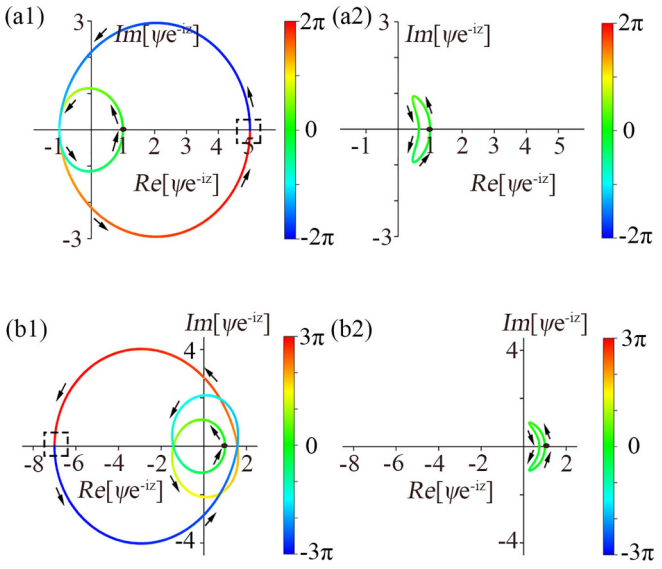

FIG. 3. (a1) and (a2) Phase-diagram trajectories of second-order RW wave function at $t = 0$ and $t = 3$, marked by I and II in Fig. 2(a). (b1) and (b2) Phase-diagram trajectories of third-order RW wave function at $t = 0$ and $t = 5$, marked by I and II in Fig. 2(c). The black dot indicates the starting and ending positions. The dashed square indicates the position of phase inversion. Black arrows indicate the direction of the track.

B. The phase of the second-order and third-order rogue waves

We further characterize the phases of high-order RWs, which admit much higher amplitude peaks and more complex phases. For the second-order RW [22,29], the maximum amplitude peak is reached at $z = 0$, and on either side of the peak there are four valleys located at $t = \pm a_{v1}, \pm a_{v2}$, which are shown in Fig. 2(a). The previous studies showed that the maximum value of a phase was π [10,12] or close to 4π [9]. But we think that the maximum phase of the RW signal is 2π, relative to the reference state's phase $\phi(t, z \to -\infty) = 0$. The second-order RW has twelve singularities on the complex plane (denoted by $m_N = a_N + ib_N$), of which the four pairs close to the real axis will collide elastically in the vertical direction at $z = 0$. The collision process can be described well by limitation analysis on vector potential. As $z \to \pm 0$, $a \to \pm a_{v1}(\pm a_{v2})$ and $b \to 0$. The vector potential on the real axis can be expressed as

$$\begin{aligned}\lim_{z\to\pm 0} \mathrm{A} = \lim_{b\to 0} \Bigg\{ & \frac{-\pi[(t\pm a_{v1})\mathbf{e}_\tau + b\mathbf{e}_t]}{2\pi[(t\pm a_{v1})^2 + b^2]} + \frac{\pi[(t\pm a_{v1})\mathbf{e}_\tau - b\mathbf{e}_t]}{2\pi[(t\pm a_{v1})^2 + b^2]} \\ & + \frac{-\pi[(t\pm a_{v2})\mathbf{e}_\tau + b\mathbf{e}_t]}{2\pi[(t\pm a_{v2})^2 + b^2]} + \frac{\pi[(t\pm a_{v2})\mathbf{e}_\tau - b\mathbf{e}_t]}{2\pi[(t\pm a_{v2})^2 + b^2]} \\ & + \frac{\pi[(t\mp a_{v1})\mathbf{e}_\tau + b\mathbf{e}_t]}{2\pi[(t\mp a_{v1})^2 + b^2]} + \frac{-\pi[(t\mp a_{v1})\mathbf{e}_\tau - b\mathbf{e}_t]}{2\pi[(t\mp a_{v1})^2 + b^2]} \\ & + \frac{\pi[(t\mp a_{v2})\mathbf{e}_\tau + b\mathbf{e}_t]}{2\pi[(t\mp a_{v2})^2 + b^2]} + \frac{-\pi[(t\mp a_{v2})\mathbf{e}_\tau - b\mathbf{e}_t]}{2\pi[(t\mp a_{v2})^2 + b^2]} \Bigg\} \\ = & (-\pi\delta[t \pm a_{v1}] - \pi\delta[t \pm a_{v2}] \\ & + \pi\delta[t \mp a_{v1}] + \pi\delta[t \mp a_{v2}])\mathbf{e}_t. \end{aligned} \tag{6}$$

The line integral of Eq. (6) along the real axis indicates that when $z \to 0$, a π ($-\pi$) phase jump occurs at $t = -a_{v1}$ (a_{v1}) and $t = -a_{v2}$ (a_{v2}). Thus, the maximum phase is indeed 2π. We plot the phase evolution of the second-order RW [shown in Fig. 2(b)], based on the general arctan $\left[\frac{\mathrm{Im}[\psi e^{-iz}]}{\mathrm{Re}[\psi e^{-iz}]}\right] + n\pi$ form, with the aid of the phase gradient flow and limitation analysis on vector potential. We can see that abrupt $2\pi \to -2\pi$ and $\pi \to -\pi$ phase jumps exist along the propagation distance for the second-order RWs, and both the RW signals and the background admit no phase changes between the initial state ($z \to -\infty$) and final state ($z \to \infty$). In contrast, the plane wave background always admits four phase jump points along the distribution direction after the highest peak emerges [9] for the identical second-order RW. Similarly, the density and phase evolution of the third-order RW [22] are shown in Figs. 2(c) and 2(d), respectively. There are three abrupt phase jumps ($3\pi \to -3\pi$, $2\pi \to -2\pi$, and $\pi \to -\pi$) along the propagation distance. We emphasize that the relative phase jumps should be taken seriously, as they play an important role in the amplitude magnification of high-order RWs.

We plot the trajectories of ψe^{-iz} and the corresponding phases at $t = 0$ (denoted by I) and $t = 3$ (denoted by II) for the second-order RW in Fig. 2(a) with propagation distance on the ($\mathrm{Re}[\psi e^{-iz}]$, $\mathrm{Im}[\psi e^{-iz}]$) plane, which are shown in Figs. 3(a1) and 3(a2). We can see that trajectory I revolves around the origin twice, and the hidden $2\pi \to -2\pi$ phase jump (marked by the black dashed square) also makes the final phase variation of the highest peak be zero, but not be 4π [9]. Meanwhile, the phase change 4π (circling around the origin twice) is hidden reasonably in the abrupt phase jump. The phase-space orbit of trajectory II in Fig. 3(a2) does

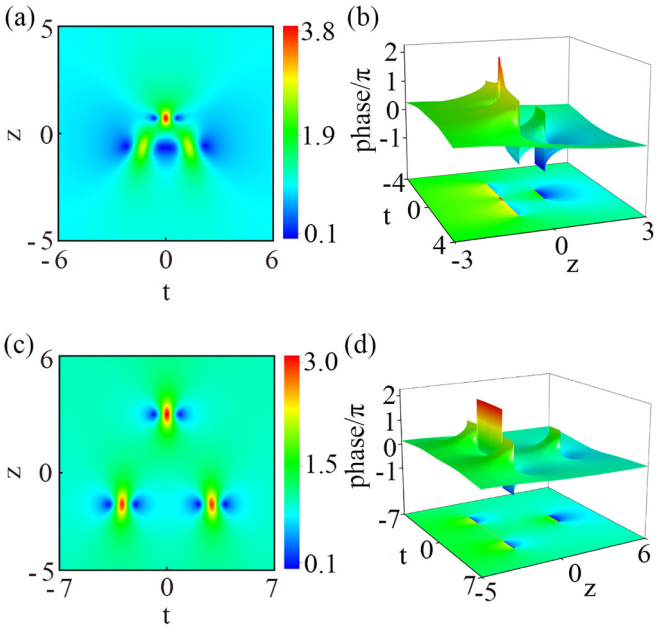

FIG. 4. (a) and (b) Amplitude and phase evolution of the second-order RW solution with the triplet structure, whose dynamics is described by Eq. (4) in Ref. [9] with the parameters being $(x_d, t_d) = (0.2, 0)$. (c) and (d) Amplitude and phase evolution of the second-order RW solution with the triplet structure, whose dynamics is described by Eq. (4) in Ref. [9] with the parameters being $(x_d, t_d) = (3, 0)$. When the three fundamental RWs separate further and further, each of them tend to admit phase evolution in Fig. 1(b). Especially, there is a small region for the 2π phase relative to the plane wave background, which is caused by the nonlinear interactions between RWs.

not encircle the origin. This indicates that the phase finally returns to the initial position and there is no phase variation for the RW's background. These characters are helpful for understanding the phase in Fig. 2(b). Trajectories I and II in Fig. 2(c) are shown in Figs. 3(b1) and 3(b2) for the third-order RW. The hidden $3\pi \to -3\pi$ phase jump is marked by the black dashed square. We can see that the plane wave background's phase also remains unchanged. This suggests that the phase difference between the initial state and final state is zero rather than $2K\pi$ (K is a nonzero integer) for high-order RWs. Similar discussions can be extended to other high-order waves on finite backgrounds [30], and the monopoles are also helpful for understanding the wavefront dislocations underlying those nonlinear waves.

The high-order RWs not only have the above polymerization structure shown in Fig. 2, but also some scattering structures. As an example, the amplitude and phase of second-order RWs with triplet structures are characterized [see Figs. 4(a) and 4(b)] based on the analytic solutions (Eq. (4) in Ref. [9]) with identical parameters in Figs. 3(c) and 3(d) in Ref. [9]. It is shown that the phase of each hump is different from the ones in Ref. [9]. When the three fundamental RWs separate well [see Figs. 4(c) and 4(d)], each of them admits phase evolution similar to the ones in Fig. 1(b). Especially, there is a small region for the 2π phase relative to the plane wave background, which is caused by the nonlinear interactions between RWs.

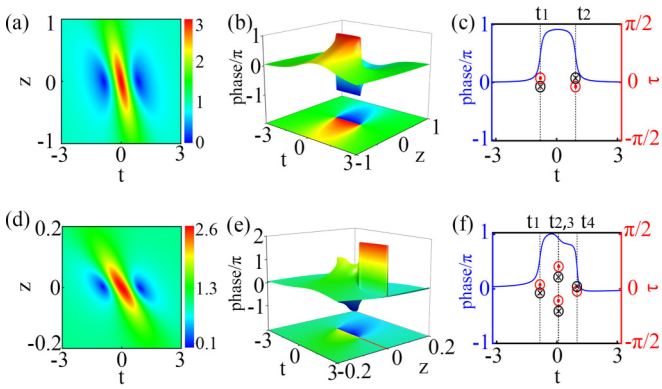

FIG. 5. (a) and (b) Amplitude and phase evolution of RW in the Hirota model with the parameter $q = 0$. (c) The phase distribution of the RW at $z = -0.1$ in the Hirota model and its corresponding virtual magnetic field on the complex plane. (d) and (e) The amplitude and phase evolution of the RW in the S-S model. (f) The phase distribution of the RW at $z = -0.01$ in the S-S model and its corresponding virtual magnetic field on the complex plane.

III. THE PHASES OF ROGUE WAVES AND RATIONAL W-SHAPED SOLITONS IN HIROTA MODEL AND SASA-SATSUMA MODEL

Taking some high-order effects, the Hirota equation and S-S equation can be used to describe the evolution of optical pulses, which have been shown to admit RW solutions and rational W-shaped solitons [31–36]. We would like to further investigate their phases. In dimensionless form, the Hirota equation can be written as

$$iE_z + \frac{1}{2}E_{tt} + |E|^2E + i\epsilon(E_{ttt} + 6|E|^2E_t) = 0. \quad (7)$$

The S-S equation [37] has also been given much attention [38–41]. In dimensionless form, it reads

$$iE_z + \frac{1}{2}E_{tt} + |E|^2E + i\epsilon(E_{ttt} + 6|E|^2E_t + 3E|E|_t^2) = 0. \quad (8)$$

The small parameter ϵ is introduced to describe the third-order dispersion, delayed nonlinear response term, and self-steeping effects (the difference between Hirota and S-S equation). If $\epsilon = 0$, Eqs. (7) and (8) reduce to the scalar NLSE. In the previous studies, the densities of RWs in these two models possess similar profiles to RW in the NLSE, with only a deflection caused by high-order effects. But the phase characteristics have not been studied. We then try to investigate the phase of RWs in Hirota and S-S equations. As an example, we choose the solutions in Refs. [32] and [34] with the parameter $\epsilon = 0.1$ to discuss the phase of RWs in the two models.

A. The phases of Rogue waves

The density and phase evolution of RWs in the two models are shown in Fig. 5 by performing the above analyzing phase method. It can be seen that the two RWs admit similar density distribution, but they have different phases. There is a small region with the 2π phase for RW in the S-S model which is absent for the Hirota model. We would like to understand their phase difference with the aid of the topological vector potentials [15]. As shown in Fig. 5(c), monopoles for the RW

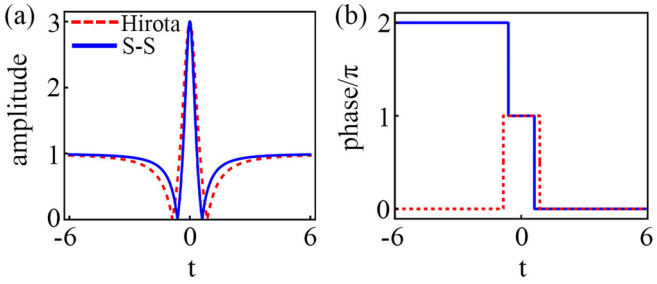

FIG. 6. (a) Amplitude distribution of W-shaped soliton in the S-S and Hirota models. (b) Corresponding phase distribution given by the limitation analysis in Fig. 7. The parameter in the Hirota model is $q = q_s$. The parameter in the S-S model is $\omega_1 = 0$.

in the Hirota model are very similar to that for NLSE [see Fig. 1(c)]. The monopole number and distribution for RW in the S-S model are different from the ones in the Hirota model, shown in Fig. 5(f). During the process of $z \to 0$, the monopole pairs for the RW in the Hirota model collide at the same propagation distance. But the monopole pairs collide at different propagation distances for RWs in the S-S model, which causes the phase to suddenly rise to 2π. The phases on the temporal-spatial plane can be used to investigate the phase evolution of the time- and space-like Peregrine breather with taking some high-order effects [11].

B. The phases of rational W-shaped solitons

We note that there are rational W-shaped soliton solutions [32,42] for the two models, which are induced by modulational stability character for the resonant perturbations. The rational W-shaped soliton solution in the Hirota model can be expressed as [33]

$$E_1 = \left[\frac{4}{1+4(t-v_s z)^2} - 1\right] e^{i\theta_s}, \tag{9}$$

where $\theta_s = q_s t - q_s^2 z/3$ and $v_s = (2+q_s^2)/(2q_s)$. The parameter q_s is the critical frequency of the plane wave background, for which the corresponding modulational instability growth rate is vanishing in the low perturbation frequency region. The rational W-shaped soliton only exists on the critical frequency. In contrast, the rational W-shaped soliton can exist in a frequency window with finite width for the S-S model [43]. It was shown that the density profile of the W-shaped soliton depends on the parameter ω_1, where $\omega_1 = \omega_0 - \frac{1}{6\epsilon}$ and ω_0 represents the frequency of the plane wave background. When $\omega_1 = 0$, its amplitude profile is almost identical to the W-shaped soliton in the Hirota model [see Fig. 6(a)]. The rational W-shaped soliton solution with $\omega_1 = 0$ in the S-S model [43] can be reduced as

$$E_2 = \left[\frac{2}{4T^2 - 2T(48z\epsilon + \sqrt{2} - 4) + M(z)} - 1\right] e^{i\theta}, \tag{10}$$

where $T = t - \frac{z}{12\epsilon}$, $M(z) = 576z^2\epsilon^2 + 24(\sqrt{2}-4)z\epsilon - 2\sqrt{2} + 5$, and $\theta = \frac{t - \frac{z}{18\epsilon}}{6\epsilon}$. We would like to further analyze their phases with ignoring the trivial phase of the plane wave background. But their phases cannot be determined uniquely, since the functions $E_1 e^{-i\theta_s}$ and $E_2 e^{-i\theta}$ are real functions with

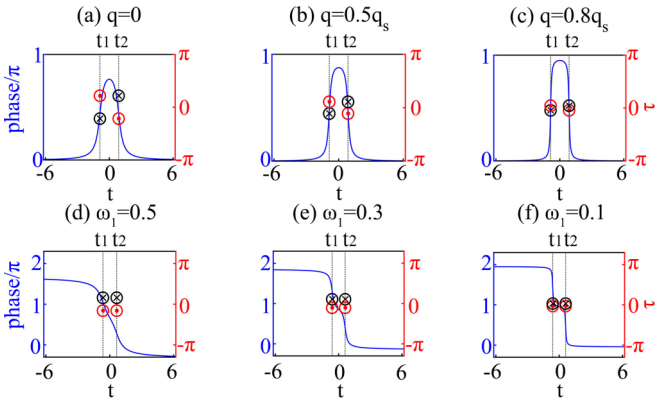

FIG. 7. (a)–(c) Virtual monopoles for RWs at $z = -0.3$ in the Hirota model with the parameter $q = 0$, $q = 0.5q_s$, and $q = 0.8q_s$, respectively. The phase of rational W-shaped solitons in the Hirota model can be given taking a limit $q \to q_s$, which predicts the red dashed line in Fig. 6(b). (d)–(f) The virtual monopoles for W-shaped solitons in the S-S model with the parameter $\omega_1 = 0.5$, $\omega_1 = 0.3$, and $\omega_1 = 0.1$, respectively. We take the limit $\omega_1 \to +0$ and predict the blue solid line in Fig. 6(b).

nodes. This is similar to the above RW with its highest peak. We suggest that their phases can be measured by approaching the precise states from proper states with no nodes. Namely, we can perform analysis on their related states with no nodes, and then take a limitation to approach them. The results are shown in Fig. 6(b). One can see that they admit quite different phases, although they admit similar density profiles. Next, we describe the analyzing process for obtaining the phases.

For the rational W-shaped soliton in the Hirota model, we choose the RW solution [32] at the distance $z = -0.3$ (slightly before its highest peak location $z = 0$) to calculate the underlying virtual monopoles. The RW solution with $z = -0.3$ admits no nodes, and it can be used to approach well the rational W-shaped soliton by varying the parameter q. We show the phases and monopoles for the RW solution with $q = 0, 0.5q_s, 0.8q_s$ in Figs. 7(a)–7(c). It is seen that there are always two pairs of monopoles with opposite charges in the (t, τ) plane. The phase of rational W-shaped soliton can be given taking a limit $q \to q_s$ [32], which is $0 \to \pi \to 0$ [the red dashed line in Fig. 6(b)]. If we approach $q = q_s$ from the RW solution at the distance slightly after its highest peak location (e.g., $z = +0.3$), the corresponding phase will become $0 \to -\pi \to 0$. By the way, the phase jumps do not depend on the approach direction of $q \to q_s$, but on whether the chosen propagation distance is before or after the RW's highest peak location. This means that rational W-shaped solitons in the Hirota model only have two possible phases from the measurement viewpoint.

For the S-S model, we choose a rational W-shaped soliton with $\omega_1 \neq 0$ to approach the case with $\omega_1 = 0$, since the RW solution cannot directly approach the rational W-shaped soliton with $\omega_1 = 0$ [43]. We take $\omega_1 = 0.5, 0.3, 0.1$ to show their phases and monopoles in Figs. 7(d)–7(f). It is seen that there are also two pairs of monopoles with opposite charges. But there are two monopoles with identical charges on the upper or lower half of the (t, τ) plane which are quite different from the cases in the Hirota model. We take the limit $\omega_1 \to +0$,

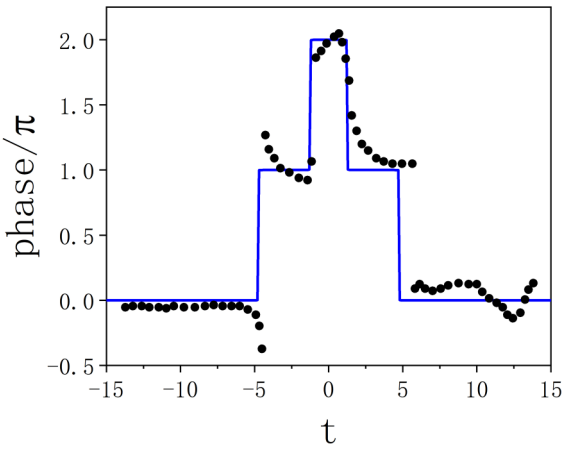

FIG. 8. The revised experimental phase profile (black circle) of the second-order RW in Ref. [10] vs our theoretical phase profile (blue solid line).

and the monopoles merge gives the phase of the rational W-shaped soliton with $\omega_1 = 0$, which is $2\pi \to \pi \to 0$ [shown by the blue solid line in Fig. 6(b)]. If we approach $\omega_1 = 0$ from $\omega_1 < 0$, the corresponding phase will be $0 \to \pi \to 2\pi$. This indicates that the rational W-shaped solitons with $\omega_1 = 0$ in the S-S model also only have two possible phases from the measurement viewpoint. Therefore, the phases of rational W-shaped solitons in the two models always show different measurement results in experiments.

IV. CONCLUSION AND DISCUSSION

By analyzing the phase gradient flow and taking the limitation analysis on vector potential, we can determine the phase evolution of nonlinear waves uniquely with choosing a reference state, based on the general arctan $\left[\frac{\mathrm{Im}[\psi]}{\mathrm{Re}[\psi]}\right] + n\pi$ form. The phase gradient flow and limitation analysis on vector potential can help us to choose the n value reasonably. This enables us to report that there is an abrupt phase jump $j\pi \to -j\pi$ ($j = 1, 2, 3$) for the jth-order RWs. The abrupt phase jumps can be used to explain both the phase and amplitude evolution of RWs, and can help to understand the differences between Refs. [8] and [9] for several identical RWs. The phase evolution in the whole temporal-spatial plane could also be helpful for understanding the phase evolution of the time- and space-like Peregrine breather [11]. We further investigate the phases of RWs and rational W-shaped solitons in the Hirota model and S-S model, for which some high-order physical effects are taken. These results show that topological vector potentials are very useful to study the phase characteristics of nonlinear waves. The phase of the Kuznetsov-Ma breather is similar to the RW's except that there are periodic oscillations along the propagation distance, and we do not show them in detail. But many efforts are still needed to address the background's phase shift of the Akhmediev breather [8], due to its periodic properties on the wave distribution direction. We expect that the background's phase shift of the Akhmediev breather should admit some more striking properties, based on our discussions on RWs' phases and our analysis of its underlying topological vector potential.

It was demonstrated that the phase of the highest peak region is identical to the continuous background for the second-order RWs in the experiments [10]. We suggest that there is a 2π phase difference between the highest peak region and the continuous background, based on the phase of the second-order RW in Fig. 2(b). The phase was measured at one propagation distance, which made the 2π and 0 phases indistinguishable. But if we measure the phase with different propagation distances, especially slightly before the highest peak emerging location, our results predict that the phase of second-order RW possesses a $0 \to \pi \to 2\pi \to \pi \to 0$ distribution (see blue solid line in Fig. 8). It is different from the ones in Fig. 4(c) in the experiments [10], but the 2π phase regime could be marked by 0 in experimental data. We cannot distinguish the 2π and 0 at a certain propagation distance, but they predict different phase gradients around the position for the highest peak. If we revise the phase experimental data of Fig. 4(c) in Ref. [10] by adding a 2π on the central 0 phase regime, the whole phase will become the black circles in Fig. 8, which agrees well with our results (see blue solid line). Based on our results, we expect that the $2\pi \to -2\pi$ and $\pi \to -\pi$ phase jumps could also be observed for the second-order RWs, if we measure the phase evolution process before and after the highest peak emerging location.

ACKNOWLEDGMENTS

We are grateful to Prof. J. Liu and Dr. X.-L. Li for their helpful discussions. This work is supported by the National Natural Science Foundation of China (Contracts No. 12022513 and No. 12235007) and the Major Basic Research Program of Natural Science of Shaanxi Province (Grant No. 2018KJXX-094).

[1] V. E. Zakharov and A. B. Shabat, Exact theory of two-dimensional self-focusing and one-dimensional self-modulation of waves in nonlinear media, Zh. Eksp. Teor. Fiz. **61**, 118 (1971).

[2] Y. S. Kivshar and B. Luther-Davies, Dark optical solitons: Physics and applications, Phys. Rep. **298**, 81 (1998).

[3] N. Akhmediev and V. I. Korneev, Modulation instability and periodic solutions of the nonlinear Schrödinger equation, Theor. Math. Phys. **69**, 1089 (1986).

[4] E. Kuznetsov, Solitons in a parametrically unstable plasma, Sov. Phys. Dokl. **22**, 507 (1977).

[5] Y. C. Ma, The perturbed plane-wave solutions of the cubic Schrödinger equation, Stud. Appl. Math. **60**, 43 (1979).

[6] D. H. Peregrine, Water waves, nonlinear Schrödinger equations and their solutions, J. Aust. Math. Soc. Ser. B **25**, 16 (1983).

[7] N. Akhmediev and A. Ankiewicz, Modulation instability, Fermi-Pasta-Ulam recurrence, rogue waves, nonlinear phase

shift, and exact solutions of the Ablowitz-Ladik equation, Phys. Rev. E **83**, 046603 (2011).
[8] N. Devine, A. Ankiewicz, G. Genty, J. M. Dudley, and N. Akhmediev, Recurrence phase shift in Fermi-Pasta-Ulam nonlinear dynamics, Phys. Lett. A **375**, 4158 (2011).
[9] D. J. Kedziora, A. Ankiewicz, and N. Akhmediev, The phase patterns of higher-order rogue waves, J. Opt. **15**, 064011 (2013).
[10] G. Xu, K. Hammani, A. Chabchoub, J. M. Dudley, B. Kibler, and C. Finot, Phase evolution of Peregrine-like breathers in optics and hydrodynamics, Phys. Rev. E **99**, 012207 (2019).
[11] Y. He, P. Suret, and A. Chabchoub, Phase evolution of the time- and space-like Peregrine breather in a laboratory, Fluids **6**, 308 (2021).
[12] A. Chowdury and W. Chang, Rogue wave fission, Phys. Rev. Res. **3**, L032060 (2021).
[13] A. Tikan, S. Bielawski, C. Szwaj, S. Randoux, and P. Suret, Single-shot measurement of phase and amplitude by using a heterodyne time-lens system and ultrafast digital time-holography, Nat. Photon. **12**, 228 (2018).
[14] A. Tikan, C. Billet, G. A. El, A. Tovbis, M. Bertola, T. Sylvestre, F. Gustave, S. Randoux, G. Genty, P. Suret, and J. M. Dudley, Universality of the Peregrine Soliton in the Focusing Dynamics of the Cubic Nonlinear Schrödinger Equation, Phys. Rev. Lett. **119**, 033901 (2017).
[15] L. C. Zhao, L.-Z. Meng, Y.-H. Qin, Z.-Y. Yang, and J. Liu, Dirac Monopoles in Rogue Waves, arXiv:2102.10914.
[16] R. Bhandari, Polarization of light and topological phases, Phys. Rep. **281**, 1 (1997).
[17] L. C. Zhao, Y. H. Qin, C. Lee, and J. Liu, Classification of dark soliton via topological vector potentials, Phys. Rev. E **103**, L040204 (2021).
[18] G. P. Agrawal, *Nonlinear Fiber Optics*, 4th ed. (Academic Press, New York, 2007).
[19] B. Kibler, J. Fatome, C. Finot, G. Millot, F. Dias, G. Genty, N. Akhmediev, and J. M. Dudley, The Peregrine soliton in nonlinear fibre optics, Nat. Phys. **6**, 790 (2010).
[20] J. M. Dudley, G. Genty, F. Dias, B. Kibler, and N. Akhmediev, Modulation instability, Akhmediev breathers and continuous wave supercontinuum generation, Opt. Express **17**, 21497 (2009).
[21] B. Kibler, J. Fatome, C. Fnot, G. Millot, G. Genty, B. Wetzel, N. Akhmediev, F. Dias, and J. M. Dudley, Observation of Kuznetsov-Ma soliton dynamics in optical fibre, Sci. Rep. **2**, 463 (2012).
[22] N. Akhmediev, A. Ankiewicz, and J. M. Soto-Crespo, Rogue waves and rational solutions of the nonlinear Schrödinger equation, Phys. Rev. E **80**, 026601 (2009).
[23] J. M. Dudley, F. Dias, M. Erkintalo, and G. Genty, Instabilities, breathers and rogue waves in optics, Nat. Photon. **8**, 755 (2014).
[24] N. Karjanto, Mathematical aspects of extreme water waves, Ph.D. thesis, University of Twente, 2006.
[25] N. Karjanto and E. van Groesen, Note on wavefront dislocation in surface water waves, Phys. Lett. A **371**, 173 (2007).
[26] Y. H. Wu, L. C. Zhao, C. Liu, Z. Y. Yang, and W. L. Yang, The topological phase of bright solitons, Phys. Lett. A **434**, 128045 (2022).
[27] Y. Ben-Aryeh, Berry and Pancharatnam topological phases of atomic and optical systems, J. Opt. B: Quantum Semiclass. Opt. **6**, R1 (2004).
[28] N. Karjanto, Peregrine soliton as a limiting behavior of the Kuznetsov-Ma and Akhmediev breathers, Front. Phys. **9**, 599767 (2021).
[29] N. Akhmediev, A. Ankiewicz, and M. Taki, Waves that appear from nowhere and disappear without a trace, Phys. Lett. A **373**, 675 (2009).
[30] N. Karjanto and E. van Groesen, Mathematical physics properties of waves on finite background, in *Handbook of Solitons: Research, Technology and Applications*, edited by S. P. Lang and S. H. Bedore (Nova Science Publishers, Hauppauge, 2009), Chap. 14, pp. 501–539.
[31] A. Ankiewicz, J. M. Soto-Crespo, and N. Akhmediev, Rogue waves and rational solutions of the Hirota equation, Phys. Rev. E **81**, 046602 (2010).
[32] The exact rational solutions in the Hirota equation [33], $E_1 = a[\frac{4+8ia^2(1-q/q_s)z}{1+4a^4(1-q/q_s)^2z^2+4a^2(t-vz)^2} - 1]e^{i\theta}$, where $v = q + (2a^2 - q^2)/(2q_s)$. The parameter q is background frequency and q_s corresponding growth rate is vanishing in the low perturbation frequency region.
[33] C. Liu, Z. Y. Yang, L. C. Zhao, and W. L. Yang, State transition induced by higher-order effects and background frequency, Phys. Rev. E **91**, 022904 (2015).
[34] S. H. Chen, Twisted rogue-wave pairs in the Sasa-Satsuma equation, Phys. Rev. E **88**, 023202 (2013).
[35] U. Bandelow and N. Akhmediev, Persistence of rogue waves in extended nonlinear Schrödinger equations: Integrable Sasa-Satsuma case, Phys. Lett. A **376**, 1558 (2012).
[36] Z. H. Li, Lu Li, H. P. Tian, and G. S. Zhou, New Types of Solitary Wave Solutions for the Higher Order Nonlinear Schrödinger Equation, Phys. Rev. Lett. **84**, 4096 (2000).
[37] N. Sasa and J. Satsuma, New-type of soliton solutions for a higher-order nonlinear Schrödinger equation, J. Phys. Soc. Jpn. **60**, 409 (1991).
[38] O. C. Wright III, Sasa-Satsuma equation, unstable plane waves and heteroclinic connections, Chaos, Solitons Fractals **33**, 374 (2007).
[39] D. Mihalache, L. Torner, F. Moldoveanu, N.-C. Panoiu, and N. Truta, Soliton solutions for a perturbed nonlinear Schrödinger equation, J. Phys. A **26**, L757 (1993).
[40] D. Mihalache, N.-C. Panoiu, F. Moldoveanu, and D.-M. Baboiu, The Riemann problem method for solving a perturbed nonlinear Schrödinger equation describing pulse propagation in optic fibres, J. Phys. A **27**, 6177 (1994).
[41] D. Mihalache, L. Torner, F. Moldoveanu, N.-C. Panoiu, and N. Truta, Inverse-scattering approach to femtosecond solitons in monomode optical fibers, Phys. Rev. E **48**, 4699 (1993).
[42] The S-S equation admits a rational W-shaped soliton solution [43], $E_2 = c\big[1 - \frac{H(t,z)}{G(t,z)}\big]e^{i\omega_0 t + iK(z)}$, with $K(z) = -\frac{\omega_1}{12\epsilon}z + \epsilon\omega_1^3 z - 6\epsilon\omega_1 c^2 z - \frac{z}{108\epsilon^2}$, where $\omega_1 = \omega_0 - \frac{1}{6\epsilon}$. The parameters ω_0 and c represent the frequency of the nonlinear background and background amplitude.
[43] L. C. Zhao, S. C. Li, and L. M. Ling, Rational W-shaped solitons on a continuous-wave background in the Sasa-Satsuma equation, Phys. Rev. E **89**, 023210 (2014).